

# Seismic Vulnerability of Low- and Mid-Rise Reinforced Concrete Buildings in Malaysia Designed by Considering Only Gravity Loads

Kok Tong Tan<sup>1</sup> · Meldi Suhatri<sup>1</sup> · Hashim Abdul Razak<sup>1</sup> · Dagang Lu<sup>2</sup>

Received: 25 March 2015 / Accepted: 11 June 2017  
© King Fahd University of Petroleum & Minerals 2017

**Abstract** This study focuses on seismic vulnerability assessment of reinforced concrete buildings designed by considering only gravity loads. Fragility curves are developed for a three-story reinforced concrete office frame building and a four-story reinforced concrete school building with unreinforced masonry infill walls representative of the essential facilities in Malaysian Peninsula. A simplified modeling approach is adopted for fragility analysis, which can effectively reduce the computational effort. A set of fragility curves are developed in terms of peak ground acceleration with lognormal cumulative distribution functions. The fragility analysis shows that the seismic performance of the structures met the desirable performance level recommended by current seismic code, demonstrating low vulnerability of the structures within Malaysian Peninsula. It is also shown that the soil condition should be taken into consideration for effective seismic vulnerability assessment. Finally, the fragility curves developed in this study are compared to those of HAZUS.

**Keywords** Seismic hazard · Artificial ground motion · Fragility curves · RC buildings · Unreinforced masonry infill walls

## 1 Introduction

Malaysian peninsula is located within a stable Sunda tectonic plate and is described by low seismicity. The main contributor to seismic hazard in Malaysian peninsula is Sumatran fault which is situated about 300–600 km away from the country [1]. However, the majority of reinforced concrete buildings in Malaysian Peninsula are designed by considering gravity and or wind loads. Damages due to 2004 Sumatra–Andaman earthquake had been reported. The earthquake felts from active Sumatran fault are also widely recorded in the recent years. Therefore, it is an urgent need to evaluate the seismic performance of the structures in order to minimize disruption and economic losses.

The objective of this study is to develop analytical fragility curves of a three-story reinforced concrete office frame buildings and a four-story reinforced concrete school buildings with unreinforced masonry infill walls. These two building types representative of the essential facilities in Malaysian Peninsula are selected and structurally modeled using fiber beam–column elements and equivalent strut. The analytical model is verified through comparison with shake table tests. The seismic responses of the structures are probabilistically estimated by considering the uncertainty in seismic demand to yield the fragility curves. The analytical fragility curves developed in this study can increase the effectiveness of seismic vulnerability assessment of essential facilities of the Malaysian Peninsula. Moreover, the structural modeling approach presented in this study can effectively reduce the computational effort. Another objective of this study is to investigate the effect of soil condition on the seismic performance of the structures. The fragility curves are developed for two different soil conditions and compared to one another. This effort shows that the soil condition should not be ignored in the effective seismic vulnerability assessment.

---

✉ Hashim Abdul Razak  
hashim@um.edu.my

<sup>1</sup> Department of Civil Engineering, University of Malaya,  
50603 Kuala Lumpur, Malaysia

<sup>2</sup> School of Civil Engineering, Harbin Institute of Technology,  
202 Haihe Road, Nangang District, Harbin 150090,  
People's Republic of China



**Fig. 1** Example of standardized school buildings in Malaysia

## 2 Structural Systems

Two representative government buildings in Malaysian Peninsula are investigated in this study: a four-story reinforced concrete school building with unreinforced masonry infill walls and a three-story reinforced concrete office frame building. In different parts of Malaysian Peninsula, the majority of these two building types have the same designs produced by Public Work Department Malaysia. The structures are designed by considering only gravity loads to meet the British Standard BS8110:1997.

In the following section, the details for each building type are described.

### 2.1 Representative School Building

The typical reinforced concrete school buildings in Malaysian Peninsula are generally composed of two main components: concrete frames and unreinforced masonry infill walls. Figure 1 shows an example of the standardized school building in Malaysia, and Fig. 2 shows the basic structural configuration in plan and elevation of the building. The structure usually is three or four stories in height and it is used as the laboratory, class room and administration office. The typical bays are 3 m long in the east–west (E–W) direction and 7.8 m long in the north–south (N–S) direction. It is symmetrical with respect to both N–S and E–W direction. The story height is 3.6 m and the slab thickness is equal to 13 cm. The class rooms are separated by unreinforced masonry infill walls. Two types of reinforcement are used for beam and column elements: ribbed bars for longitudinal reinforcement and plain bars for transverse reinforcement. Table 1 summarizes the material properties of the structure. Moreover, a super-imposed live load of  $3.0 \text{ kN/m}^2$  is applied to the structure. A nominal value of  $2.0 \text{ kN/m}^2$  for super-imposed dead load is considered for concrete tiles, ceiling, cold formed, insulation and mechanical and electrical services.

### 2.2 Representative Office Building

The typical reinforced concrete office buildings in the region are generally composed of concrete moment frames. Figure 3 shows the typical structural configuration in plan and elevation of the structure along with member sizes. The number of stories of the structure usually ranges from two to three stories in height. The typical bays are 8 m long in the E–W direction and either 1.0 m or 0.6 m long in the N–S direction. It is also symmetrical with respect to both N–S and E–W directions. The story height is 4.0 m and the slab thickness is equal to 15 cm. The material properties of the structure are listed in Table 1. A super-imposed dead and live load of  $2.0 \text{ kN/m}^2$  and  $2.5 \text{ kN/m}^2$  is applied to the structure. All these parameters are extracted from as-built drawings produced by Public Work Department Malaysia.

### 2.3 Finite-Element Model

Three-dimensional finite-element models were generated using the OpenSees [2] platform. The column and beam elements were simulated with distributed plasticity and fiber-based section element. The cross sections of beam and column elements were divided into unconfined cover concrete, confined core concrete and steel fibers with corresponding material stress–strain relationships. The modified Kent and Park [3] model was used to model the concrete cyclic behavior. This model allows an accurate prediction of the structural demand for flexure-dominated RC members despite its relatively simple formulation [4,5]. The modified Menegotto and Pinto [6] model with isotropic strain hardening was employed to model the reinforcing steel behavior. This model has sufficient accuracy to satisfy the experimental tests and takes into account the Bauschinger effect [7]. The DOF coupling feature of OpenSees [2] was used to define the rigid floor diaphragm. The column base is fixed, while shear deformation and bond slip of reinforcement were neglected. The effects of gravity loads and second-order effects were included in the analysis through the consideration of geometric nonlinearities.

For unreinforced masonry infill walls, a single equivalent diagonal strut proposed by Kadysiewski and Mosalam [8] was adopted. The strut does not carry any vertical loads, and the out-of-plane behavior of the strut is modeled using the arching mechanism [9]. The effect of partially infilled walls for openings was not taken into account. Inelastic dynamic time history analyses were performed using the artificially generated ground motions. A 2% of critical damping was used in the analytical model as suggested by [10]. The artificial ground motions are applied in the N–S direction parallel to the unreinforced masonry infill walls.

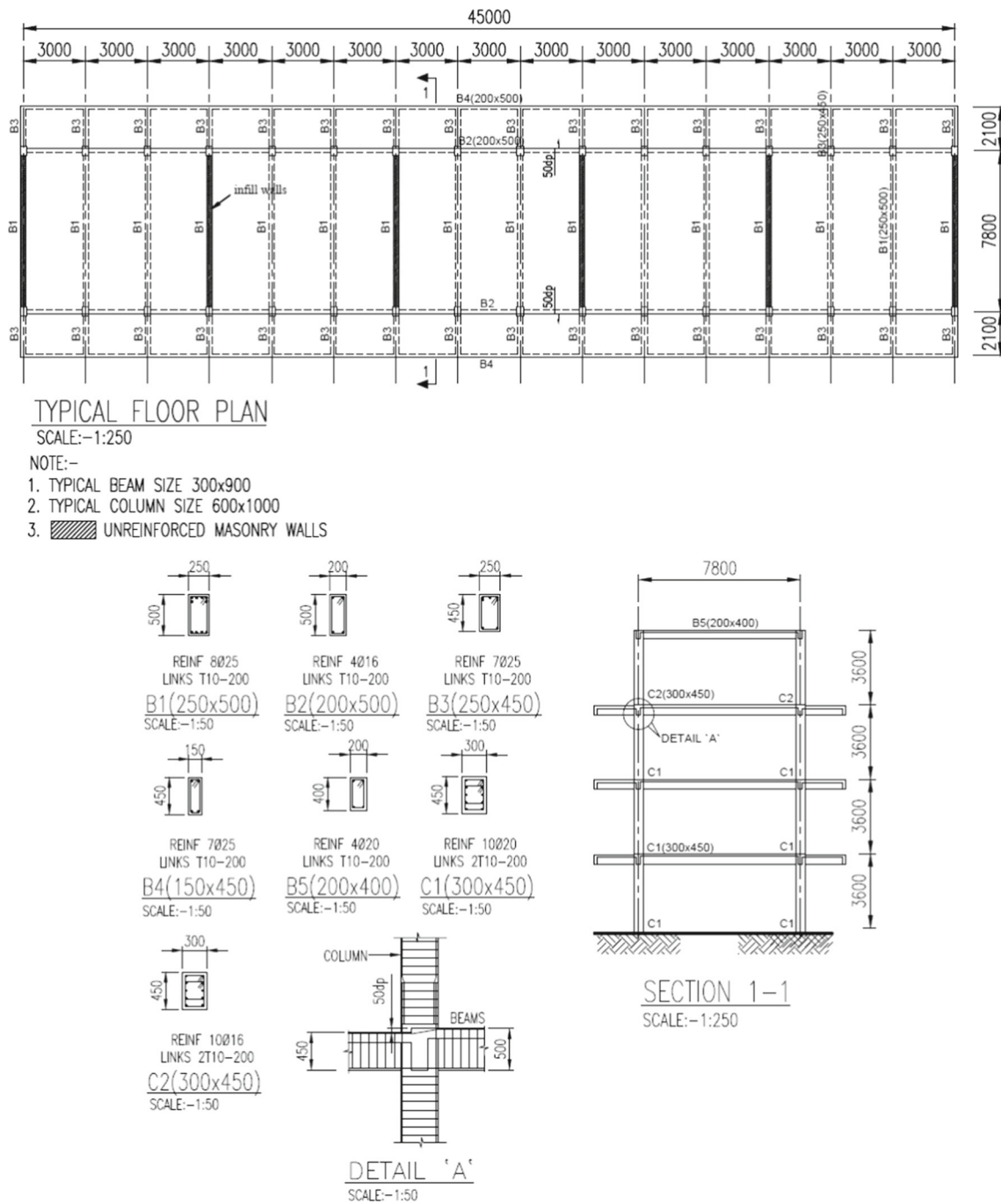


Fig. 2 Basic structural configuration in plan and elevation view of school building along with its member sizes

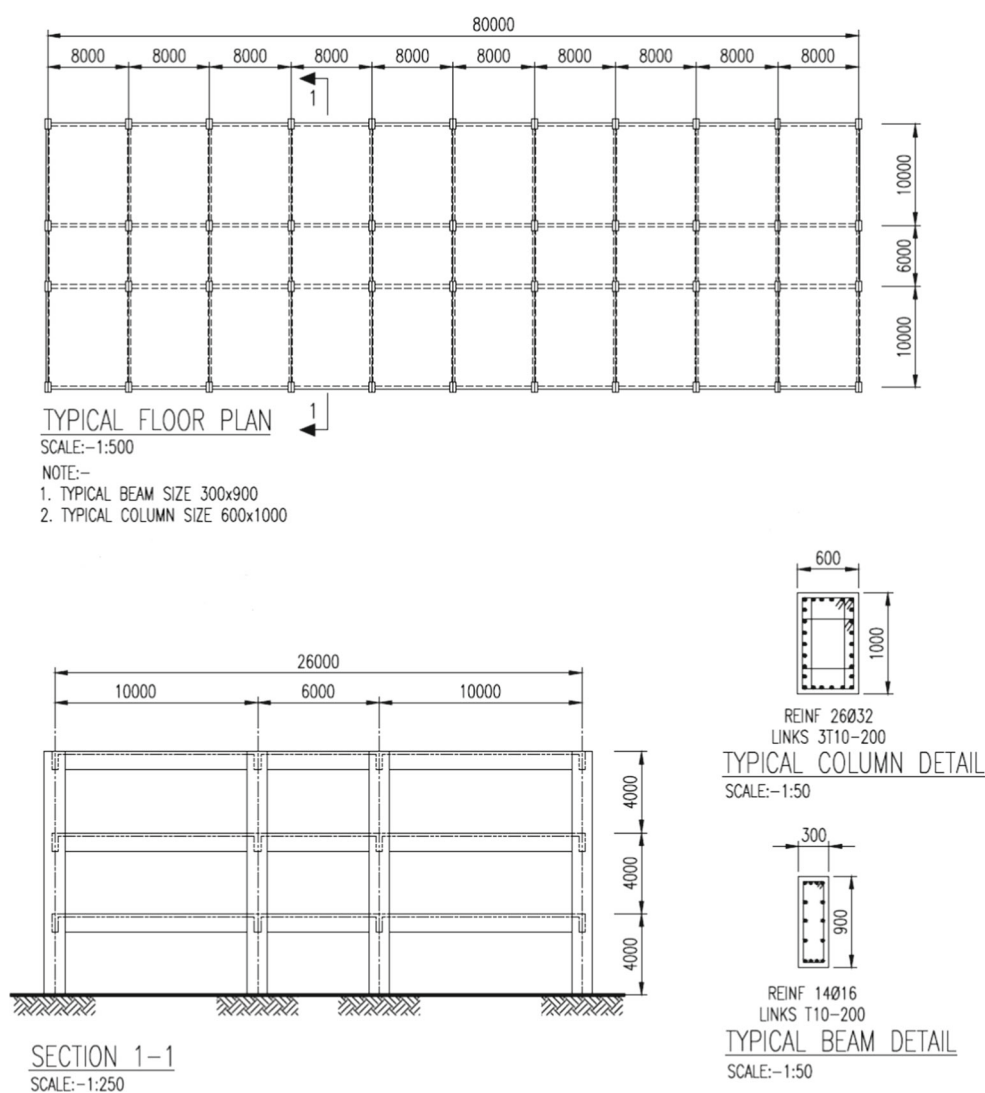
Some researchers [11–13] have shown that the material uncertainty has a relatively smaller effect on the fragility functions as compared to ground motion variability. Therefore, the material properties of the structures are simulated based on its mean values as presented in Table 1. The differences of the seismic action with respect to soil conditions are selected in this study to derive representative fragility functions.

### 3 Verification of Analytical Model

The analytical model for four-story reinforced concrete school building with unreinforced masonry infill walls is validated through comparison of time history analysis with shake table test conducted by [14]. The validation is undertaken in terms of global acceleration and displacement time histories.

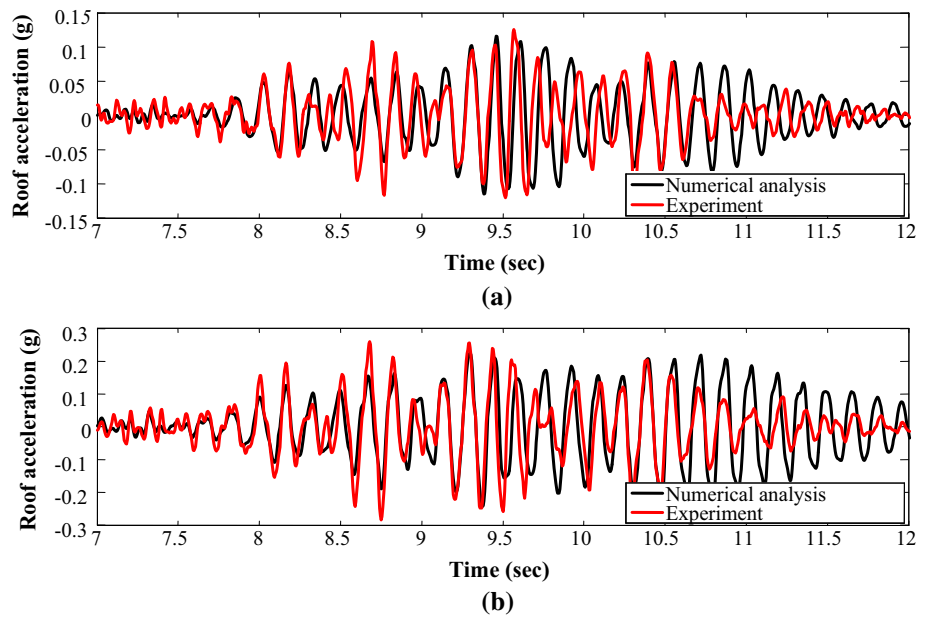
**Table 1** Material properties of the structures

Properties	School building with unreinforced masonry infill walls	Office frame building
Mean concrete compressive cube strength (MPa)	30	30
Mean yield stress of longitudinal reinforcement—ribbed bar (MPa)	500	500
Mean yield stress of transverse reinforcement—plain bar (MPa)	250	250
Mean density of masonry (kN/m <sup>3</sup> )	15	—
Mean masonry compressive strength (MPa)	10.00	—
Mean masonry elastic modulus (MPa)	3440	—
Mean masonry bed-joint shear strength (MPa)	0.15	—

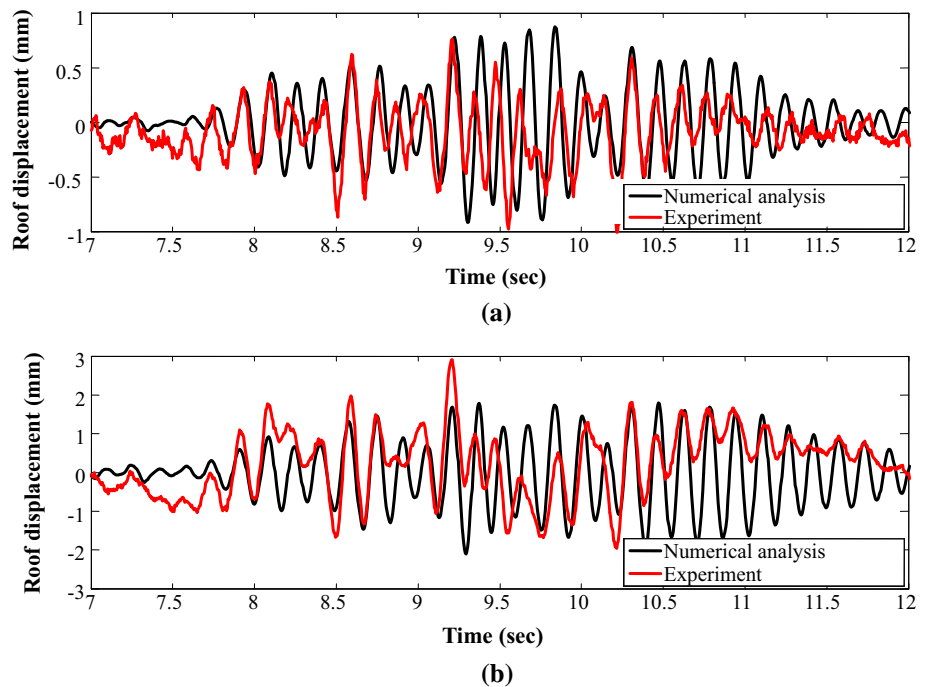


**Fig. 3** Typical structural configuration in plan and elevation view of office building along with its member sizes

**Fig. 4** Comparison of dynamic analysis for school building: **a** roof acceleration at PGA of 0.06 g and **b** roof acceleration at PGA of 0.12 g [14]



**Fig. 5** Comparison of dynamic analysis for school building: **a** roof displacement at PGA of 0.06 g and **b** roof displacement at PGA of 0.12 g [14]



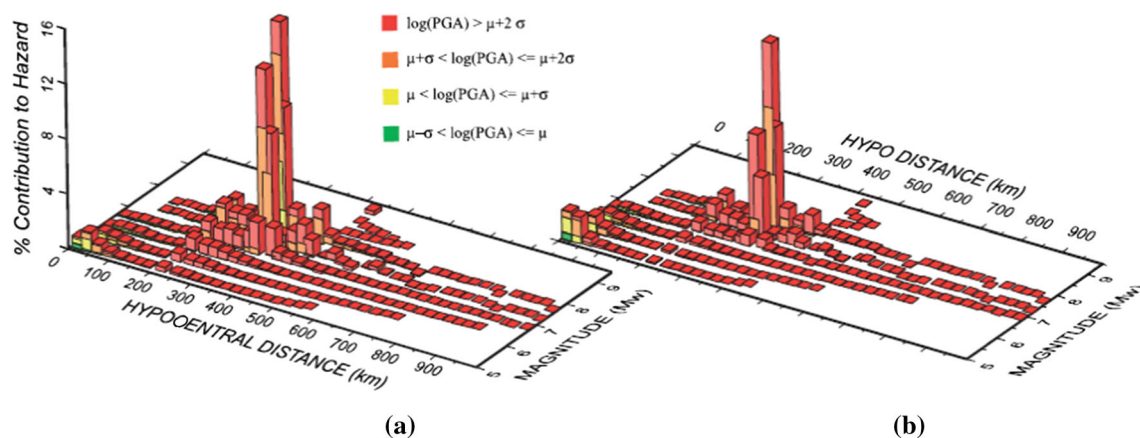
### 3.1 Acceleration Response History Validation

Figure 4 shows the comparison of the roof story acceleration of the 1:2 scale model and analysis using a 1:2 scale analytical model. It can be seen that the analytical results show good agreement with the experimental results until about 10.5 s, but after that, the analytical model shows considerably larger values. This is probably caused by the discrepancy in damping characteristics of the analytical model and test structure. The damping ratio of the test structure is apparently greater than that of the analytical model. The roof accelerations of the

analytical model are about 10–20% larger than those of the experimental test. This is because the finite-element model is based on assumptions of the element stiffness and boundary conditions, and the actual response of the structure cannot be determined accurately.

### 3.2 Displacement Response History Validation

Figure 5 shows the comparison of the roof story displacement of the 1:2 scaled model and analysis using a 1:2 scale analytical model. As seen, the analytical result also shows good



**Fig. 6** Dominating earthquake scenarios: **a** 10/50 PE and **b** 2/50 PE [1]

agreement with the experimental result up to 10.5 s. This is also due to the difference in damping characteristics of the analytical model and test structure. Overall, the analytical values are about 10–25% larger than those of the experimental test which shows the analytical model is of good accuracy.

#### 4 Input Ground Motions

In this study, ground motion records are selected based on earthquake magnitude and hypocentral distance. [1] showed that the earthquakes with magnitude of 7.7 and distance of 323 km are contributing most to the site hazard through deaggregation as shown in Fig. 6. Several seismic codes [15, 16] and studies [17, 18] recommended that at least seven acceleration time histories must be applied to the structure to be allowed to use average results instead of the most unfavorable ones. A set of twelve ground motion records are then selected from the Consortium of Organizations for Strong Motion Observation Systems [19] Strong Motion Database, which is more than the recommendation for vulnerability analysis. The following criteria are also considered in the selection process.

- (i) The magnitude of the event of the selected time histories should be within the range of  $M_w \pm 0.20M_w$  [20].
- (ii) The distance of the event of the selected time histories should be more than 100 km.
- (iii) The selected time histories are either from sites underlain by geologic rock or from stiff soils.

Different records are considered in the selection process in order to include the inherent uncertainties related to the seismic motion such as seismotectonic environment, amplitude, frequency content and significant duration. No rupture directivity effect is taken into account, and local ground responses are evaluated through numerical analyses where the seismic

motion is applied in outcrop condition at the base of soil columns. Three target spectra of Kuala Lumpur corresponding to 50, 10 and 2% probabilities of exceedance in 50 years, derived by [21], are selected to be used in spectrum matching of the selected ground motions. This is to account for spectral shapes with different intensity levels.

The spectrum-matched records were generated using enhanced RspMatch [22] program. Enhanced RspMatch modifies a given record to render it compatible with a given spectrum while preserving the nonstationary character of the ground motion. Table 2 lists the source parameters of the selected records. Both horizontal components of the acceleration records were employed to produce 24 earthquake events for each hazard level. The artificial ground motions on the surface are then generated using one-dimensional equivalent linear approach, which is based on the assumption of vertical propagation of seismic waves and horizontal soil layering.

Two typical soil conditions are investigated in this study. The first one is soil class D which has a shear wave velocity of 277 m/s. The second one is soil class E with shear wave velocity of 171 m/s. The soil stratigraphy and the corresponding shear wave velocity values are shown in Fig. 7. The site response analysis is conducted using SHAKE91 [23]. The modulus reduction and damping curves (Fig. 8) proposed by Darendeli [24] and Schnabel et al. [25] were adopted for soil and bedrock, respectively. Furthermore, the effective strain to maximum shear strain was assumed to be 65% and initial hysteretic damping ratio was taken as 5%. Figure 9 shows three plots for the selected record: 1—original, 2—matched and 3—site-dependent spectra against target spectrum. Figure 10 shows the maximum acceleration distribution along the depth for soil class D and E. It can be seen that the peak ground accelerations at soil class D are about 18–50% higher than those at soil class E. Consequently, the soil class D is contributing the higher PGA than the soil class E.

**Table 2** Selected records and their source parameters

Earthquake name	Year	Station name	$M_w$	Hyp. depth (km)	$R_{rup}$ (km)	$V_{s30}$ (m/s)
Chi-Chi, Taiwan	1999	KAU003	7.62	6.76	114.4	913.8
Near the south coast of Honshu	2004	NARH01	7.40	44	158.3	>1500
Near the south coast of Honshu	2004	WKYH02	7.40	44	177.3	>1500
Off the coast of northern California	2005	USGS 1584	7.10	10	132.9	>760
Western Tottori	2000	YMGH05	7.30	11	178.3	>1500
Duzce, Turkey	1999	KOER769	7.10	10	183.5	>760
Landers, CA	1992	CSMIP 23590	7.30	7.0	121.1	>760
Landers, CA	1992	CSMIP 23595	7.30	7.0	145.1	>760
Uttarkashi, India	1991	ALMO	7.01	10.0	153.5	>760
India–Burma border	1988	CHER	7.21	90.0	353.0	>760
India–Burma border	1988	MAWK	7.21	90.0	379.6	>760
India–Burma border	1988	UMMU	7.21	90.0	314.5	>760

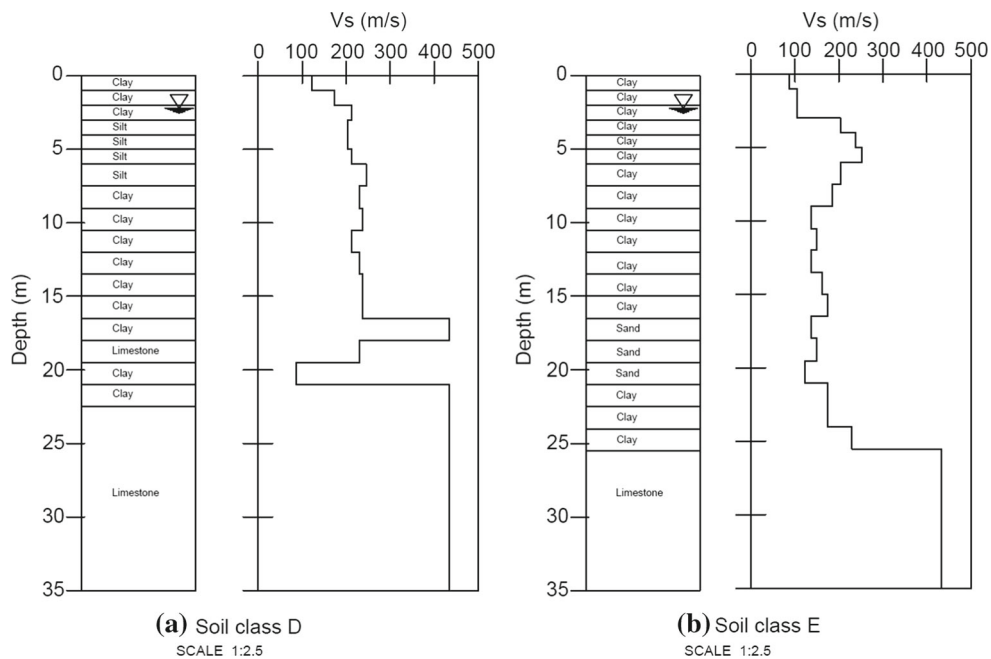


**Fig. 7** Typical soil stratigraphy and shear wave velocity values for soil class D and E

### 5 Performance Levels

In order to carry out a comparison with fragility curves from the literature, the same definition of damage levels must be considered. HAZUS [26] provides definition of damage levels and fragility curves for classes of buildings depending on building type, seismic design level and building height. Four different damage levels, namely slight, moderate, extensive and complete damage states, were proposed. Maximum inter-story drift ratio was used as a damage measure, and each damage level has a threshold value of inter-story drift ratio. In this study, the damage states and the associated drift ratios proposed for low-rise concrete moment frame building (CIL)

and mid-rise concrete frame with unreinforced masonry infill walls (C3M) and pre-code design level are adopted, which are summarized in Tables 3 and 4, respectively. For concrete moment-resisting frames, the slight damage shows flexural or shear hairline cracks at beam–column joints. The maximum tension stress of concrete and yield stress of reinforcement steel (lengthwise) are expected. The moderate damage expects the hairline cracks to be extent to most beam and column elements. However, some elements in ductile frames show larger flexural cracks and concrete cover spalling. The extensive damage shows larger flexural cracks, concrete spalling and main reinforcement buckling. Strength degradation of core concrete can be seen. The complete

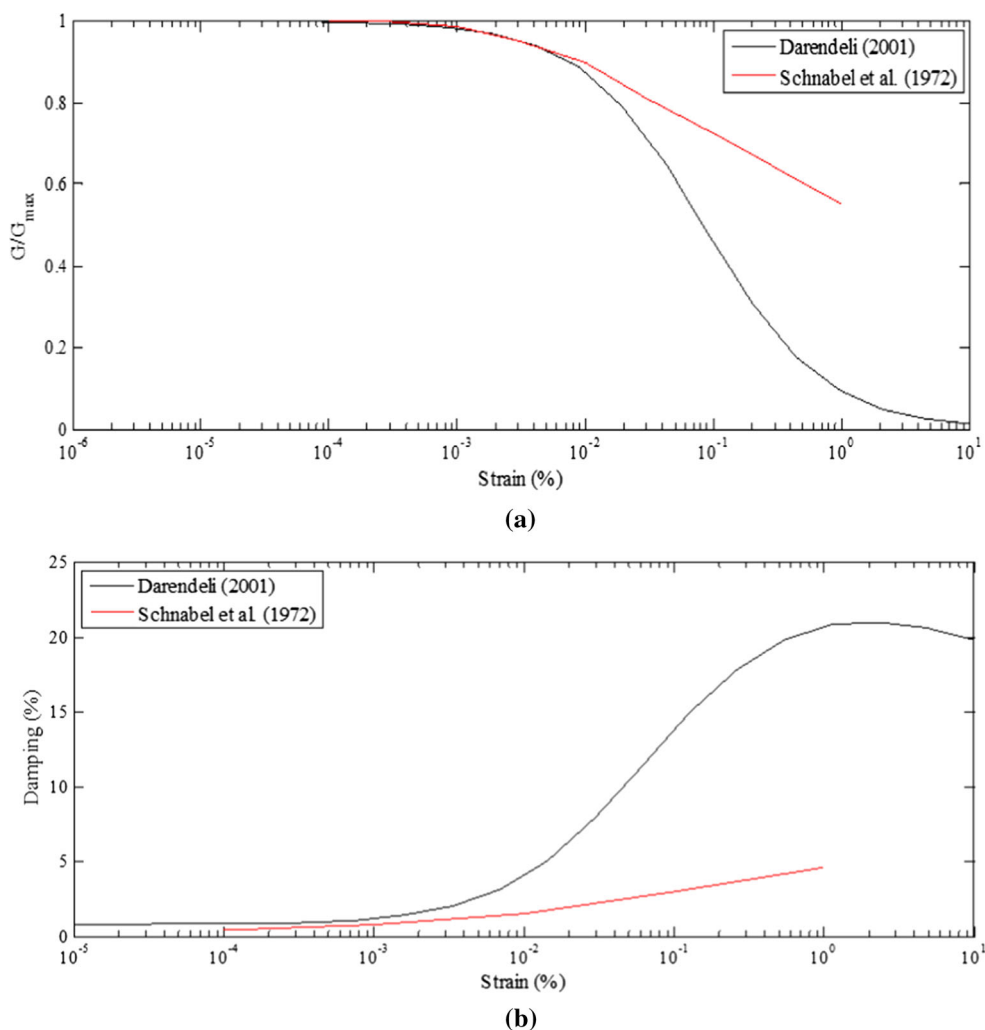


Fig. 8 Dynamic soil properties: a modulus reduction curves and b damping curve

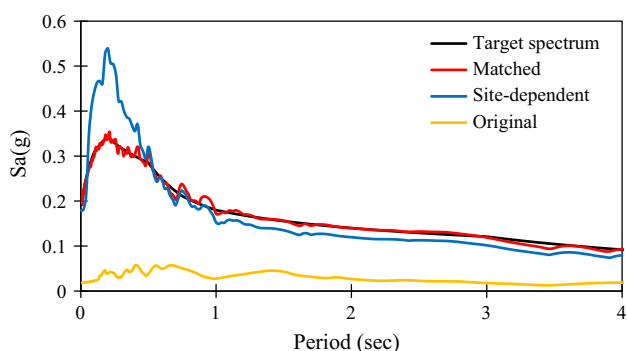


Fig. 9 Three plots for the selected record: 1—original, 2—matched and 3—site-dependent spectra against target spectrum

damage shows the structure collapsed and lost its stability. Ultimate strain of longitudinal reinforcement bars (steel failure) and confined core concrete (transverse rebar failure) can be easily observed.

For concrete frames with unreinforced masonry infill walls, the slight damage shows cracks on most infill walls. The moderate damage expects limited crushing of bricks at beam-column joints, while the extensive damage shows the walls partially or fully fell and the complete damage expects the walls have completely disintegrated. Therefore, the fragility curves are developed accordingly and compared to those of HAZUS [26].

### 6 Fragility Curves

Seismic fragility analysis by means of fragility curves determines the conditional probability that the structure has a state of damage exceeding the damage state  $d_i$  at a given earthquake intensity- level PGA and is usually defined using

$$P [D > d |PGA] = P [X > x_i |PGA]$$

**Fig. 10** Maximum acceleration distribution along the depth of soil class D and E for input motion of: **a** 0.15 g, **b** 0.75 g and **c** 1.0 g

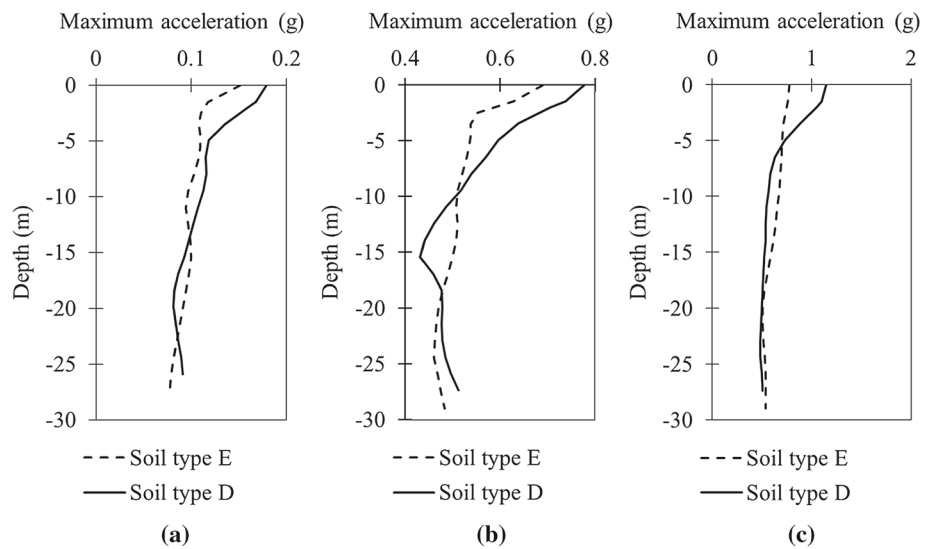


**Table 3** Structural performance levels for low-rise concrete moment frame (C1L) with pre-code design-level HAZUS [26]

Structural performance levels				
	Slight damage	Moderate damage	Extensive damage	Complete damage
Overall damage descriptions	Flexural or shear-type hairline cracks in some beams and columns near joints or within joints. Maximum tension stress of concrete and yield stress of reinforcement steel (lengthwise)	Most beams and columns show hairline cracks. Some elements in ductile frames have reached yield capacity indicated by larger flexural cracks and some concrete cover spalling. Nonductile frames may exhibit larger shear cracks and spalling	Some frame elements in ductile frames have reached their ultimate capacity indicated by large flexural cracks, spalled concrete and buckled main reinforcement. Nonductile frame elements may suffer shear failures or bond failures at reinforcement splices, or broken ties or buckled main reinforcement in columns which may result in partial collapse. Strength degradation of core concrete	Structure is collapsed or in imminent danger of collapse due to brittle failure of nonductile frame elements or loss of frame stability. Ultimate strain of longitudinal steel bars (steel failure) and confined core concrete (transverse rebar failure)
Drift ratio (%)	0.4	0.64	1.6	4.0

**Table 4** Structural performance levels for mid-rise concrete frame with unreinforced masonry infill walls (C3M) and pre-code design-level HAZUS [26]

Structural performance levels				
	Slight damage	Moderate damage	Extensive damage	Complete damage
Overall damage descriptions	Diagonal (sometimes horizontal) hairline cracks on most infill walls; cracks at frame–infill interfaces	Most infill wall surfaces exhibit larger diagonal or horizontal cracks; some walls show crushing of brick around beam–column joints. Diagonal shear cracks may be observed in concrete beams or columns	Most infill walls exhibit large cracks; some bricks may dislodge and fall; some infill walls may bulge out-of-plane; few walls may fall partially or fully; few concrete columns or beams may fail in shear resulting in partial collapse. Structure may show permanent lateral deformation	Structure has collapsed or is in imminent danger of collapse due to a combination of total failure of the infill walls and nonductile failure of beams and columns
Drift ratio (%)	0.16	0.32	0.80	1.87

1.0 Criteria for damage states										
SLIGHT MODE. EXT. COMP.										
Drift limit, x <sub>i</sub> :	0.004	0.0064	0.016	0.04						
2.0 Response matrix R [i,j]										
PGA (g)	0.1	0.2	0.3	0.4	0.5	0.6	0.7	0.8	0.9	
Event	Inter-story drift ratio									
EQ1-ew	0.0005	0.0011	0.0016	0.0022	0.0028	0.0034	0.0041	0.0047	0.0053	
EQ1-ns	0.0005	0.001	0.0015	0.0021	0.0026	0.0031	0.0037	0.0042	0.0048	
EQ2-ew	0.0005	0.0011	0.0016	0.0022	0.0027	0.0033	0.0038	0.0044	0.005	
EQ2-ns	0.0004	0.0008	0.0013	0.0017	0.0022	0.0026	0.0031	0.0035	0.004	
⋮	⋮	⋮	⋮	⋮	⋮	⋮	⋮	⋮	⋮	
EQ11-ns	0.0028	0.0055	0.0078	0.01	0.0114	0.0142	0.0173	0.0201	0.0219	
EQ12-ew	0.0027	0.0056	0.0079	0.0095	0.0114	0.0128	0.0134	0.0146	0.0161	
EQ12-ns	0.0023	0.0051	0.0082	0.0104	0.0109	0.0115	0.0161	0.02	0.0225	
Assumption of LOGNORMAL distribution										
σ	0.0009	0.0018	0.0026	0.0031	0.0035	0.004	0.0045	0.0051	0.0056	NOTE: STDEV(R[:,j])
μ	0.0014	0.0029	0.0043	0.0054	0.0065	0.0076	0.0086	0.0096	0.0106	AVERAGE (R[:,j])
δ	0.6288	0.6264	0.6063	0.5708	0.5383	0.5303	0.5292	0.5296	0.5331	σ/μ
β (slope)	0.3332	0.331	0.313	0.282	0.2544	0.2478	0.2469	0.2473	0.2501	Eq. (3): ln(1+δ <sup>2</sup> )
α (interse)	-6.596	-5.894	-5.503	-5.253	-5.075	-4.916	-4.788	-4.68	-4.582	Eq.(2): ln(μ)-0.5β <sup>2</sup>
3.0 Fragility analysis										
Eq. (1): $P[D > d   PGA] = P[X > x_i   PGA] = 1 - \Phi \left[ \frac{\ln(x_i) - \alpha}{\beta} \right]$										
Fragility = 1-NORMSDIST ((ln(xi)-α)/β)										
SLIGHT	0.0006	0.1304	0.5231	0.8293	0.9605	0.9927	0.9985	0.9997	0.9999	
MODERATE	2E-06	0.0055	0.0744	0.2372	0.4639	0.7074	0.8573	0.9332	0.9698	
EXTENSIVE	8E-14	5E-08	6E-06	4E-05	0.0001	0.0008	0.0041	0.0137	0.0371	
COMPLETE	0	0	1E-13	3E-13	2E-13	4E-12	1E-10	2E-09	3E-08	
4.0 Simplified fragility curves										
4.1 Fitting to lognormal distribution										
Eq. (6): $Z = \Phi^{-1} [F_A(a)] = \text{NORMALSINV}(\text{fragility})$										
ln(PGA)	-2.303	-1.609	-1.204	-0.916	-0.693	-0.511	-0.357	-0.223	-0.105	
Z(Slight)	-3.224	-1.124	0.0579	0.9513	1.7566	2.4427	2.9718	3.4012	3.7567	
Z(Moderat)	-4.635	-2.544	-1.443	-0.715	-0.091	0.5459	1.0685	1.5004	1.8778	
Z(Extensiv)	-7.385	-5.312	-4.37	-3.964	-3.692	-3.152	-2.642	-2.205	-1.785	
Z(Comple)			-7.298	-7.213	-7.293	-6.85	-6.353	-5.911	-5.448	
4.2 Lognormal distribution parameters										
Damage sta	ζ <sub>A</sub>	LN(m <sub>A</sub> )	NOTE:							
Slight	0.311	-1.26	ζ <sub>A</sub> = INDEX (LINEST (:),1)							
Moderate	0.3407	-0.712	LN (m <sub>A</sub> ) = INDEX (LINEST (:),2)							
Extensive	0.4136	0.7058								
Complete	0.4753	2.5757								

Fig. 11 Example of the derivation of the fragility functions

**Table 5** Parameters of the fragility functions

Damage state	School buildings				Office buildings			
	Soil class D		Soil class E		Soil class D		Soil class E	
	$m_A$ (g)	$\xi_A$	$m_A$ (g)	$\xi_A$	$m_A$ (g)	$\xi_A$	$m_A$ (g)	$\xi_A$
Slight	0.2222	-2.7651	0.2391	-2.0738	0.311	-1.2599	0.3176	-1.3154
Moderate	0.2362	-2.0813	0.2261	-1.3272	0.3407	-0.7122	0.3557	-0.7503
Extensive	0.2199	-1.1251	0.2147	-0.4547	0.4136	0.7058	0.4584	0.8384
Complete	0.2123	-0.3441	0.1927	0.2306	0.4753	2.5757	0.5921	3.3689

$$= 1 - \Phi \left[ \frac{\ln(x_i) - \alpha}{\beta} \right] \tag{1}$$

$$\alpha = \ln \mu - \frac{1}{2} \beta^2 \tag{2}$$

$$\beta = \sqrt{\ln \left[ 1 + \left( \frac{\sigma}{\mu} \right)^2 \right]} \tag{3}$$

where  $\Phi(\cdot)$  is the standard normal cumulative distribution function,  $x_i$  is the upper bound for each damage state ( $d_i$ ;  $i$  = slight, moderate, extensive and complete) as presented in Tables 3 and 4,  $\alpha$  and  $\beta$  as defined in Eqs. (2) and (3) are dependent on the PGA level,  $\sigma$  and  $\mu$  are, respectively, the mean and standard deviation of seismic demand values given in each PGA level.

In this way, the fragility curves of the structure corresponding to different limit states can be obtained by plotting the PGA level and the probability of exceeding limit states. As common practice, the fragility curves are also fitted to the lognormal cumulative distribution functions as follows:

$$F_A(a) = \Phi(Z) \tag{4}$$

and  $Z$  is the standard normal variable, which is expressed as

$$Z = \frac{[\ln(a) - \ln(m_A)]}{\xi_A} \tag{5}$$

where  $A$  is the random variable of the PGA,  $m_A$  is the median of  $A$ , and  $\xi_A$  is the logarithmic standard deviation of  $A$ . The standard normal variable can be estimated using the following expression:

$$Z = \Phi^{-1}[F_A(a)] \tag{6}$$

where  $\Phi^{-1}(\cdot)$  is the inverse function of the standard normal cumulative distribution. The parameters of the fragility function can be estimated by plotting the standard normal variable against  $\ln(\text{PGA})$  values. The median and logarithmic standard deviation of  $A$  ( $m_A, \xi_A$ ) are then estimated from the  $y$ -intercept and the slope of the fitted line, respectively. The 5 and 95% of confidence levels are estimated using the following expressions:

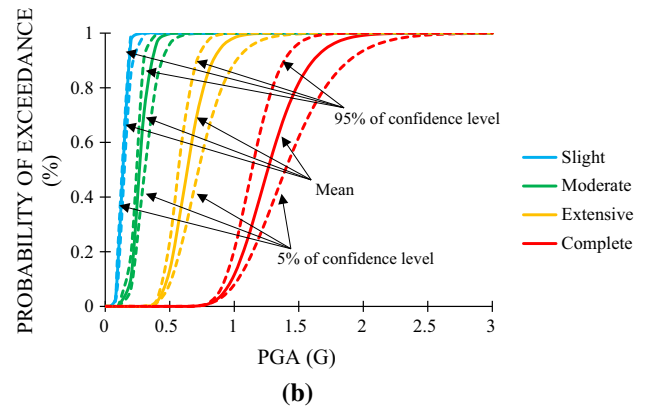
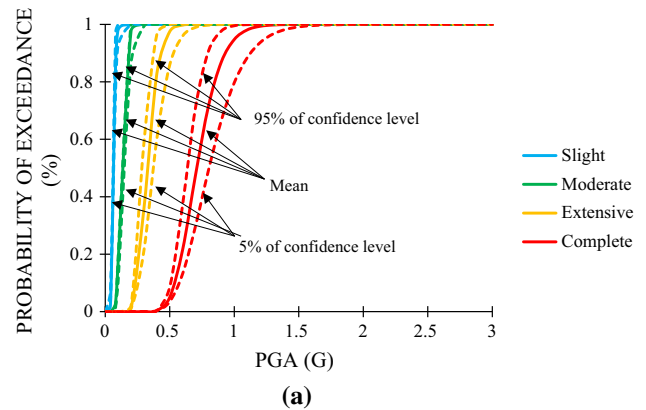


**Fig. 12** Fragility curves of school building with 5 and 95% of confidence levels: **a** soil class D and **b** soil class E

$$\mu_{95\%} = \mu + 1.96\sigma/\sqrt{n} \tag{7}$$

$$\mu_{5\%} = \mu - 1.96\sigma/\sqrt{n} \tag{8}$$

Figure 11 shows an example step by step for constructing the fragility curve of office building. Table 5 summarizes the parameters of the fragility function for the structures. Figures 12 and 13 show the fragility curves for the structures at soil class D and E along with 5 and 95% of confidence levels.

Figure 14 compares the fragility curves between the soil class D and E for the structures. It is observed that overall the soil class D shows higher probability of exceeding a damage state over the soil class E. For school building, the probability of exceeding the extensive damage is increased from 13%

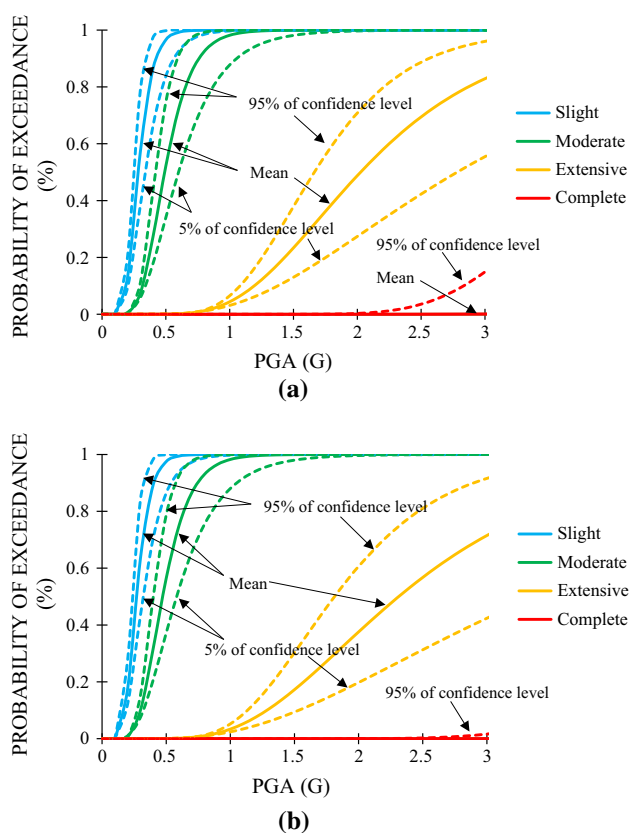


**Fig. 13** Fragility curves of office building with 5 and 95% of confidence levels: **a** soil class D and **b** soil class E

(soil class E) to about 95% (soil class E) at a PGA level of 0.5 g, whereas the complete damage is up to 90% (soil class D) from 11% (soil class E at a PGA level of 1 g. For office building, the probability of exceeding the extensive damage is increased from 37% (soil class E) to approximately 50% (soil class D) at a PGA level of 2 g. However, the slight and moderate damage states of office building are not much different. Despite the lower damage limits of office building, the difference of the fragility function for higher damage limits of office building and school building is quite noticeable. This shows that the fragility function of the structures is sensitive to soil conditions. Therefore, the soil conditions should be taken into account for effective seismic vulnerability assessment of reinforced concrete buildings with or without unreinforced masonry infill walls.

Furthermore, [1] have shown that the peak ground acceleration at 2 and 10% probability of exceedance in 50 years is about 0.12 and 0.2 g, respectively. The probability of exceeding various limit states for the structures is then read from the fragility curves. Table 6 summarizes the probability of exceeding limit states for different hazard levels. The seismic performance of the structures observed from Fig. 14 and Table 6 is compared to the performance level suggested by the current seismic code to measure its rela-

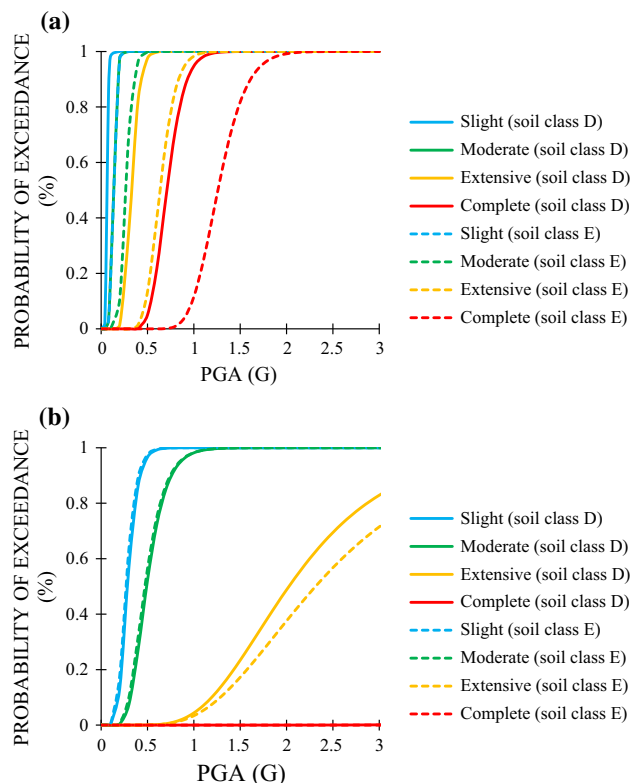


**Fig. 14** Comparison of fragility curves between soil class D and E: **a** school building and **b** office building

tive vulnerability. Among others, [9] defines three seismic performance levels—basic safety objective, enhanced rehabilitation objectives and limited rehabilitation objectives. Each performance level is achieved using one or a combination of two methods. In this study, the basic safety objective performance level defined in [9] is adopted, which is to ensure the life safety level and collapse prevention level for the earthquake level of 10/50 and 2/50 PE, respectively. Based on the damage descriptions and drift limits shown in Tables 3 and 4, it can be stated that the life safety and collapse prevention level defined in [9] are consistent with the moderate and extensive damage of HAZUS [26], respectively. For both soil conditions, the structures show less than 20% probability of exceeding the moderate damage for the earthquake level of 10/50 PE and less than 5% probability of exceeding the extensive damage for the earthquake level of 2/50 PE. Therefore, the seismic performance of the structures met the desirable building performance level recommended by the seismic code, indicating low vulnerability of the structures within Malaysian Peninsula.

## 7 Fragility Comparison

The fragility curves of the structures developed in this study are compared to the HAZUS [26] fragility curves. The com-

**Table 6** Probability of exceeding limit states for different earthquake levels

Building function	Soil class	Earthquake level (prob. of exceed.)	PGA (g)	Probability of exceeding limit states			
				Slight	Moderate	Extensive	Complete
School	D	10% in 50 years	0.12	0.981	0.174	0.000	0.000
		2% in 50 years	0.20	0.100	0.977	0.014	0.000
	E	10% in 50 years	0.12	0.169	0.000	0.000	0.000
		2% in 50 years	0.20	0.974	0.106	0.000	0.000
Office	D	10% in 50 years	0.12	0.000	0.000	0.000	0.000
		2% in 50 years	0.20	0.131	0.004	0.000	0.000
	E	10% in 50 years	0.12	0.000	0.000	0.000	0.000
		2% in 50 years	0.20	0.177	0.008	0.000	0.000

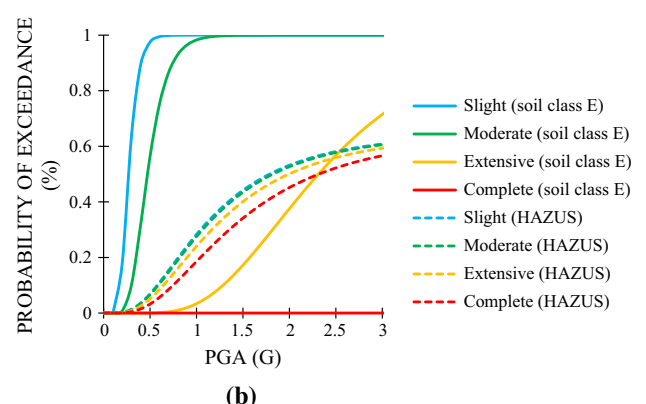
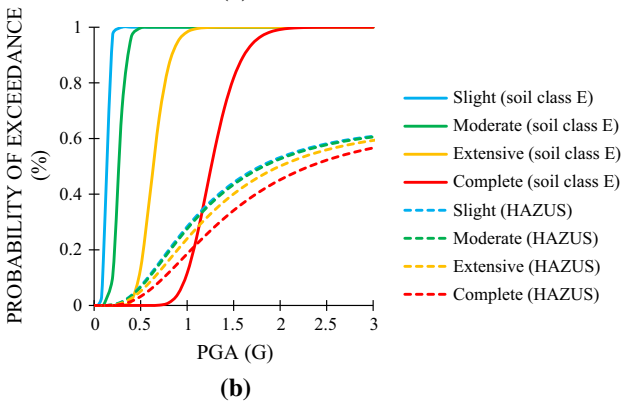
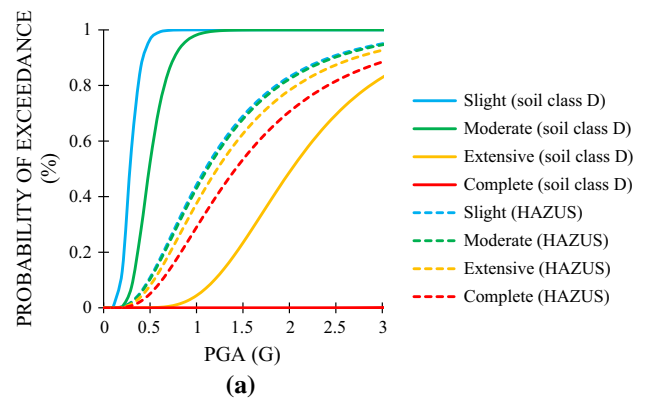
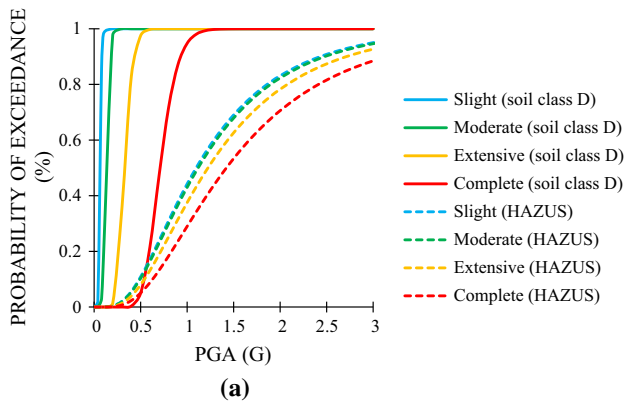


**Fig. 15** Comparison of fragility curves for school building with HAZUS: **a** soil class D and **b** soil class E

**Fig. 16** Comparison of fragility curves for office frame building with HAZUS: **a** soil class D and **b** soil class E

parison is shown for the HAZUS-equivalent PGA fragility curves developed for pre-code low-rise concrete moment frame (C1L) and pre-code mid-rise concrete frame with unreinforced masonry infill walls, since the structures investigated are designed by considering only gravity loads. For the comparison, the equivalent PGA functions of HAZUS are adjusted to account for earthquake magnitude, source-to-site distance and site condition. Figures 15 and 16 show the comparison of the fragility curves of the structures at different sites and those of HAZUS. It can be seen that the

fragility curves of the structures developed in this study are generally higher than those of HAZUS except the extensive and complete damage states of low-rise reinforced concrete frame building. The discrepancy is probably due to different source of data used in the generation of fragility curves. The fragility curves presented in HAZUS are derived using lognormal distribution parameters that are defined based on expert judgment, while the fragility curves developed in this study are based on damage distributions simulated from the time history analyses.

## 8 Conclusions

Analytical fragility curves for a three-story reinforced concrete office frame building and a four-story reinforced concrete school building with unreinforced masonry infill walls were developed in this study. A simplified model was developed based on fiber beam–column element and equivalent strut to describe the critical inelastic behavior of the structures in an effective manner. The analytical model shows a good agreement with shake table tests. The fragility curves were then developed for the structures by considering the uncertainty in seismic demand.

The fragility analysis shows that the seismic performance of the structures met the desirable performance level recommended by the current seismic code, indicating low vulnerability of the structures within Malaysian Peninsula. It is also shown that the soil condition should be taken into consideration for effective seismic vulnerability assessment of reinforced concrete buildings with or without unreinforced masonry infill walls. Moreover, the analytical fragility curves developed in this study show higher probability of exceeding a limit state than those of HAZUS. This is probably due to different source of data used in the generation of fragility curves.

**Acknowledgements** The research presented in this paper was funded by the postgraduate research fund of University of Malaya, Project PV081-2011A. Special thanks are due to UNESCO and the People's Republic of China for supporting the first author to Harbin Institute of Technology (HIT) from September 2011 to August 2012 via the UNESCO/China (The Great Wall) Co-Sponsored Fellowships Programme.

## References

- Petersen, M.D.; Dewey, J.; Hartzell, S.; Mueller, C.; Harmsen, S.; Frankel, A.D.; et al.: Probabilistic seismic hazard analysis for Sumatra, Indonesia and across the Southern Malaysian Peninsula. *Tectonophysics* **390**, 141–158 (2004)
- Mazzoni, S.; McKenna, F.; Scott, M.H.; Fenves, G.L.: *OpenSees command language manual—version 2.0*. University of California, Berkeley (2007)
- Kent, D.C.; Park, R.: Flexural members with confined concrete. *J. Struct. Div.* **97**, 1969–1990 (1971)
- Lagaros, N.D.; Papadrakakis, M.: Neural network based prediction schemes of the non-linear seismic response of 3D buildings. *Adv. Eng. Softw.* **44**, 92–115 (2012)
- Mitropoulou, C.C.; Papadrakakis, M.: Developing fragility curves based on neural network IDA predictions. *Eng. Struct.* **33**, 3409–3421 (2011)
- Menegotto, M.; Pinto, P.E.: Method of analysis for cyclically loaded reinforced concrete plane frames including changes in geometry and non-elastic behavior of elements under combined normal force and bending. In: *Symposium on Resistance and Ultimate Deformability of Structures Acted on by Well Defined Repeated Loads*, pp. 15–22. IABSE, Lisbon (1973)
- Li, Z.; Hatzigeorgiou, G.D.: Seismic damage analysis of RC structures using fiber beam-column elements. *Soil Dyn. Earthq. Eng.* **32**, 103–110 (2012)
- Kadysiewski, S.; Mosalam, K.M.: Modeling of unreinforced masonry infill walls considering in-plane and out-of-plane interaction. PEER report 2008/102 Pacific Earthquake Engineering Research Center College of Engineering, University of California, Berkeley (2009)
- Fema 356: *Prestandard and Commentary for the Seismic Rehabilitation of Buildings*. Federal Emergency Management Agency, Washington DC (2000)
- Kwon, O.S.; Kim, E.: Case study: analytical investigation on the failure of a two-story RC building damaged during the 2007 Pisco-Chincha earthquake. *Eng. Struct.* **32**, 1876–1887 (2010)
- Kwon, O.-S.; Elnashai, A.: The effect of material and ground motion uncertainty on the seismic vulnerability curves of RC structure. *Eng. Struct.* **28**, 289–303 (2006)
- Jeong, S.-H.; Elnashai, A.S.: Probabilistic fragility analysis parameterized by fundamental response quantities. *Eng. Struct.* **29**, 1238–1251 (2007)
- Ellingwood, B.R.; Kinali, K.: Quantifying and communicating uncertainty in seismic risk assessment. *Struct. Saf.* **31**, 179–187 (2009)
- Tan, K.T.; Abdul, R.H.; Lu, D.; Li, Y.: Seismic response of a four-storey RC school building with masonry-infilled walls. *Nat. Hazards* **78**, 141–153 (2015)
- BS EN 1998-1. Eurocode 8: Design of Structures for Earthquake Resistance. Part 1: General Rules, Seismic Actions and Rules for Buildings (2004)
- UBC. Structural Engineering Design Provision. In: *International Conference of Building Officials* (1997)
- Bommer, J.J.; Acevedo, A.; Douglas, J.: The selection and scaling of real earthquake accelerograms for use in seismic design and assessment. In: *Proceedings of ACI International Conference on Seismic Bridge Design and Retrofit*, American Concrete Institute (2003)
- Huang, Y.; Whittaker, A.; Luco, N.; Hamburger, R.: Scaling earthquake ground motions for performance-based assessment of buildings. *J. Struct. Eng.* **137**, 311–321 (2009)
- Consortium of Organizations for Strong Motion Observation Systems (COSMOS). <http://www.strongmotioncenter.org/vdc/scripts/search.plx>
- Bommer, J.J.; Acevedo, A.: The use of real earthquake accelerograms as input to dynamic analysis. *J. Earthq. Eng.* **8**, 43–91 (2004)
- Engineering Seismology and Earthquake Engineering Research Center (ESEER). Seismic hazard assessment of Kuala Lumpur and Kedah. Skudai, University of Technology Malaysia, Johor (2013)
- Atik, L.A.; Abrahamson, N.: An improved method for nonstationary spectral matching. *Earthq. Spectra* **26**, 601–617 (2010)
- Idriss, I.M.; Sun, J.I.: SHAKE91: A Computer Program for Conducting Equivalent Linear Seismic Response Analyses of Horizontally Layered Soil Deposits. University of California, Davis, California (1992)
- Darendeli, M.B.: Development of a New Family of Normalized Modulus Reduction and Material Damping Curves. The University of Texas at Austin (2001)
- Schnabel, P.B.; Lysmer, J.; Seed, H.B.: SHAKE: A Computer Program for Earthquake Response Analysis of Horizontally Layered Sites. Report no EERC72-12. University of California, Berkeley (1972)
- HAZUS. HAZUS-MH MR4 Technical Manual. Department of Homeland Security Emergency Preparedness and Response Directorate FEMA (2003)

